Chemistry–A European Journal
Research Article
doi.org/10.1002/chem.202302063
Chemistry Europe
European Chemical Societies Publishing
www.chemeurj.org

Hot Paper

Closed Synthetic Cycle for Nickel-Based Dihydrogen Formation

Soosan Hosseinmardi,[a] Andreas Scheurer,[a] Frank W. Heinemann,[a] Nicola Marigo,[b] Dominik Munz,*[b] and Karsten Meyer*[a]

Dedicated to Professor Herbert W. Roesky on the occasion of his 88th birthday

Dihydrogen evolution was observed in a two-step protonation reaction starting from a Ni^0 precursor with a tripodal N-heterocyclic carbene (NHC) ligand. Upon the first protonation, a Ni^{II} monohydride complex was formed, which was isolated and fully characterized. Subsequent protonation yields H_2 via a transient intermediate (INT) and an isolable Ni^{II} acetonitrile complex. The latter can be reduced to regenerate its Ni^0 precursor. The mechanism of H_2 formation was investigated by using a deuterated acid and scrutinized by ^{1}H NMR spectroscopy and gas chromatography. Remarkably, the second protonation forms a rare nickel dihydrogen complex, which was detected and identified in solution and characterized by ^{1}H NMR spectroscopy. DFT-based computational analyses were employed to propose a reaction profile and a molecular structure of the Ni–H_2 complex. Thus, a dihydrogen-evolving, closed-synthetic cycle is reported with a rare Ni–H_2 species as a key intermediate.

Introduction

Hydrogen (H_2) is an appealing alternative to carbon-based fuels, and, in this context, the hydrogen economy has given considerable attention to metal hydrides.[1–4] While cobalt complexes have been extensively studied for hydrogen production,[5–16] nickel hydride complexes, obtained by protonation of the corresponding Ni^0 complex,[17–22] are currently attracting interest due to their potential to transfer protons, hydrogen atoms, or hydrides.[23–27] In H_2 evolution chemistry, molecular Ni hydride catalysts are known for H_2 production through proton reduction.[4,27–30] In this regard, the chemistry of Ni hydride complexes is also becoming increasingly important because of their role in nickel-containing enzymes. In [NiFe]-hydrogenases' active site, a Ni hydride species is proposed to be a crucial intermediate in the biological process of hydrogen metabolism, *viz.*, the generation and consumption of H_2.[31–35]

Herein, we report the synthesis and study of a chelating tris-carbene-based Ni complex that produces H_2 upon two sequential protonations. In this system, the N-heterocyclic carbene ligand is our first- generation *tris*-[2-(3-isopropylimidazol-2-ylidene)ethyl]-amine (TIMEN^{iPr}) chelate.

Results and Discussion

Previously, our group reported a Ni^0 *tris*-NHC derivative with *tert*-butyl substituents, namely [Ni(TIMEN^{tBu})].[36] In [Ni(TIMEN^{tBu})], the more encumbering *tert*-butyl groups engage the electron-rich Ni^0 center in three Ni···H anagostic interactions, thus, effectively shutting down any further reactivity. Considering the sterically less demanding *iso*-propyl substituents, the present ligand system provides a more open coordination sphere that leads to a significantly more reactive Ni^0 complex.

Accordingly, the zero-valent nickel complex, [Ni(TIMEN^{iPr})] (**1**), was prepared by the reaction of [Ni(COD)$_2$] with one equivalent of TIMEN^{iPr} in cold tetrahydrofuran. The red powder was isolated and characterized by ^{1}H and ^{13}C NMR spectroscopy and showed a diamagnetic behavior (Figures S7–S13 in the Supporting Information). Red crystals of **1**, suitable for a single-crystal X-ray diffraction (sc-XRD) study, were obtained from a *n*-hexane solution of **1** at −35 °C (Figure 1, left). Neutral **1** crystallized with two independent molecules of the complex and half a molecule of *n*-hexane in its asymmetric unit. In one of the two independent complex molecules, one of the ligand's *i*Pr groups was disordered (Figure S41). The geometry of the Ni center's first coordination sphere in **1** is best described as trigonal planar with the nickel center located slightly below the plane of the three carbene carbon ligands towards the N-anchor (out-of-plane shift, $U_{oop} = -0.0204(9)$ Å for Ni(1) and

[a] S. Hosseinmardi, Dr. A. Scheurer, Dr. F. W. Heinemann, Prof. Dr. K. Meyer
Department of Chemistry and Pharmacy, Inorganic Chemistry
Friedrich-Alexander-Universität Erlangen-Nürnberg (FAU)
Egerlandstraße 1, 91058 Erlangen (Germany)
E-mail: karsten.meyer@fau.de

[b] N. Marigo, Prof. Dr. D. Munz
Inorganic Chemistry: Coordination Chemistry
Saarland University
Campus C4.1, 66123 Saarbrücken (Germany)
E-mail: dominik.munz@uni-saarland.de

Supporting information for this article is available on the WWW under https://doi.org/10.1002/chem.202302063

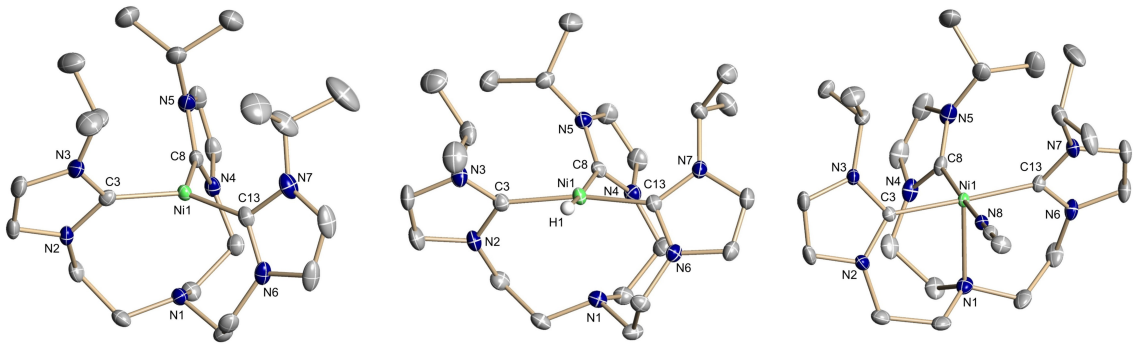

Figure 1. Thermal ellipsoid representations at the 50% probability level of the molecular structures of neutral **1** (left), cation $\mathbf{2}^{+}$ (middle), and dication $\mathbf{3}^{2+}$ (right) in crystals of **1**•0.25 C_6H_{14}, **2** (PF_6), and **3** $(BPh_4)_2$. Hydrogen atoms (except for the hydride in $\mathbf{2}^{+}$), solvent molecules (except for coordinated acetonitrile in $\mathbf{3}^{2+}$), and counter anions are omitted for clarity.

−0.0400(9) Å for Ni(2)). The Ni–C bond distances were determined at Ni(1)–C(3) = 1.8824(15) Å, Ni(1)–C(8) = 1.8782(15) Å, Ni(1)–C(13) = 1.8692(15) Å, and Ni(2)–C(27) = 1.8678(14) Å, Ni(2)–C(32) = 1.8664(15) Å, and Ni(2)–C(37) = 1.8789(14) Å; hence, the average Ni–C bond lengths of 1.877(2) Å and 1.871(2) Å in the two independent molecules is 1.874(2) Å. Lastly, the amine nitrogen anchor in **1** remains non-coordinating at a Ni–N_{anchor} distance of 2.6698(13) Å for Ni(1)–N(1) and 2.6063(13) Å for Ni(2)–N(8). For comparison, the Ni–C bond lengths in [Ni(TIMEN^{tBu})] are equivalent with 1.892(1) Å, which is slightly longer due to an increased steric crowding at the Ni center compared with the *iso*-propyl derivative.[36] Also, the Ni–N_{anchor} distance of 3.204 Å in [Ni(TIMEN^{tBu})] is significantly longer and excludes Ni–N_{anchor} interaction. As noted above, the electron-rich nickel center and one hydrogen atom of each of the three *tert*-butyl groups show anagostic interactions with Ni···HC distances of 2.611 Å (d(Ni–C_{tBu}) = 3.379 Å).[36] The distance between the central nickel atom and the *iso*-propyl hydrogens in [Ni(TIMEN^{iPr})] is, on average, 2.871 and 2.883 Å in the two crystallographically independent molecules, suggestive of no such interactions in **1**.

The addition of [2,6-lutidinium](BPh_4) to a solution of **1** in tetrahydrofuran at room temperature leads to a rapid reaction, indicated by a change in color from red to yellow. The formation of a hydride complex, [(TIMEN^{iPr})Ni(H)](BPh_4), **2** (BPh_4), is confirmed by a resonance signal in the ^{1}H NMR spectrum at $\delta = -14.36$ ppm in CD_3CN. According to ^{1}H NMR and ^{13}C NMR spectroscopy, complex $\mathbf{2}^{+}$ displays diamagnetism (Figures S14–S19). The molecular structure of [(TIMEN^{iPr})Ni(H)]$^{+}$, $\mathbf{2}^{+}$, in crystals of its hexafluorophosphate salt, was also determined by sc-XRD (Figure 1, middle, Figure S42). Yellow crystals of complex **2** (PF_6), suitable for a sc-XRD study, were obtained by slow diffusion of Et_2O into a THF solution of **2** (PF_6). The monohydride [(TIMEN^{iPr})Ni(H)]$^{+}$, $\mathbf{2}^{+}$, features a distorted square planar geometry with a τ_4 geometry index value of 0.19,[37] and the hydride shifted up by 0.39(4) Å out of the *tris*-carbene plane. The position of this hydridic H atom (H1) was taken from a difference Fourier synthesis, and its positional parameters were refined without restrictions, resulting in a Ni–H bond length of 1.61(4) Å. This value agrees well with the only other reported neutron crystal structure of a nickel complex having terminal hydride ligands, where the Ni–H distances were determined at 1.592, 1.640, and 1.611 Å.[38] Furthermore, the Ni–C(3), Ni–C(8), and Ni–C(13) distances in **2** (PF_6) are 1.901(3), 1.937(3), and 1.892(3) Å, respectively, with the longest one, Ni–C(8), *trans* to the hydride. Also, the Ni–N_{anchor} distance in **2** (PF_6) was determined at 2.747(3) Å and the anchor is – similar to zero-valent **1** – considered non-coordinating. Moreover, $(\mathbf{2})^{+}$ features C(3)–Ni–H and C(13)–Ni–H angles of 84(2)° and 81(2)°, as well as C(3)–Ni–C(8) and C(13)–Ni–C(8) angles of 100.39(12)° and 95.20(12)°, respectively.

Subsequently, by adding another equivalent of the lutidinium salt to the Ni^{II} hydride solution, $\mathbf{2}^{+}$, the yellow color intensifies, H_2 bubbles appear, and a new Ni species [(TIMEN^{iPr})Ni(NCCH$_3$)]$^{2+}$, $\mathbf{3}^{2+}$, is formed. The evolution of H_2 can be detected as a characteristic singlet resonance at $\delta =$ 4.55 ppm in the ^{1}H NMR spectrum of $\mathbf{2}^{+}$ in [D_8]THF (Figure S27).[39] Dihydrogen formation was further confirmed by gas chromatography (GC) with a thermal conductivity detector (TCD, see the Supporting Information). To verify the origin of the evolved H_2, [[D]-2,6-lutidinium](BPh_4) was prepared for protonation. HD production is confirmed when $[Hlut]^{+}$ is used as the first proton source, while $[Dlut]^{+}$ is used as the second (Figure S37). This observation affirms the protonation of the Ni^0 complex to form the nickel hydride, which then produces HD upon the addition of D^{+} to the solution of $\mathbf{2}^{+}$. Next, $[Dlut]^{+}$ was used as the only proton source and, accordingly, D_2 gas could be detected; additional formation of HD is explained by the $[Hlut]^{+}$ impurity in $[Dlut]^{+}$ that has been confirmed by ^{1}H NMR spectroscopy. Thus, the production of H_2 through a nickel hydride complex is fully supported. Moreover, to prove the quantitative formation of H_2, the evolved gas was collected with a gastight syringe and analyzed by GC-TCD, thereby confirming that the yield of H_2 exceeds 86% (see the Supporting Information).

Yellow crystals of [(TIMEN^{iPr})Ni(NCCH$_3$)]$(BPh_4)_2$ (**3** $(BPh_4)_2$) were obtained by slow evaporation of an acetonitrile solution of $\mathbf{3}^{2+}$, and the solid-state structure of **3** $(BPh_4)_2$ was determined by sc-XRD (Figure 1, right). In dicationic $\mathbf{3}^{2+}$, the Ni ion is five-coordinate in a C_3N_2 ligand environment, in which the central Ni ion possesses a distorted square pyramidal geometry. The three individual Ni–C_{NHC} bond distances are equivalent within

the 3-σ-criterion, giving an average Ni–C_{NHC} bond length of 1.911(2) Å. In addition to the chelate's three carbene carbons, one acetonitrile molecule is bound in the equatorial position (d(Ni–N_{CH3CN}) = 1.8986(10) Å), thus, replacing the hydride. In contrast to **1** and $\mathbf{2}^+$, the N-anchor is now coordinated to Ni with d(Ni–N_{anchor}) = 2.3917(11) Å. Moreover, the yellow powder was isolated and characterized by ^{1}H and ^{13}C NMR spectroscopy and showed a diamagnetic behavior (Figures S20–S26).

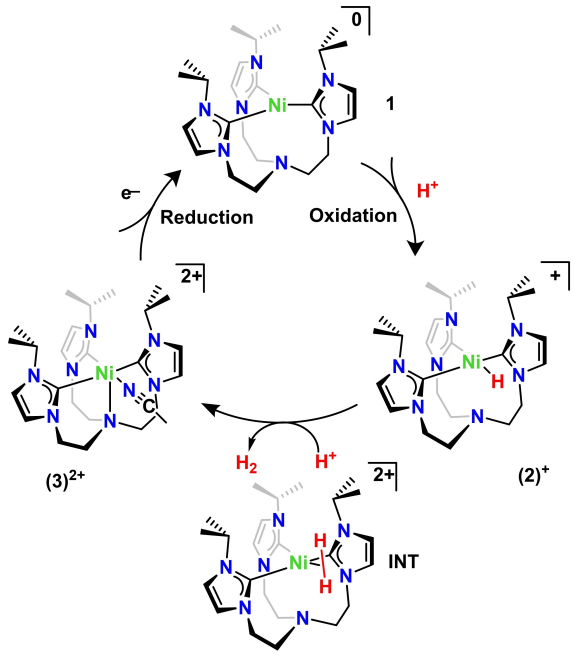

Figure 2. Synthetic cycle for Ni-based H_2 formation from H^+.

Owing to the gradual reaction between nickel hydride $(\mathbf{2})^+$ and protons in THF solvent, an intermediate was detected in the reaction solution by ^{1}H NMR spectroscopy. Accordingly, a variable-temperature (VT) NMR study was set up to follow the reaction (Figures S28 and S29). To a frozen solution of compound **1** in [D_8]THF, 2.5 equiv. of [2,6-lutidinium](BPh_4) in cold [D_8]THF were added, immediately frozen, and subjected to an NMR experiment at −80 °C. During the second protonation step, the resonance at ≈ −14.3 ppm, assigned to the hydride in $\mathbf{2}^+$, starts decreasing in intensity, while a new resonance at ≈ −22.3 ppm appears and increases over the temperature range from −20 to +20 °C. After full conversion, the resonance at ≈ −22.3 ppm begins decreasing again, and the formation of the diamagnetic Ni^{II} complex, $(\mathbf{3}^{THF})^{2+}$, is observed (+40 °C). Clearly, the resonance at ≈ −22.3 ppm originates from an intermediate species (**INT**), which forms upon the reaction of hydride $\mathbf{2}^+$ with a proton and before the evolution of H_2 gas with the formation of $(\mathbf{3}^{THF})^{2+}$. At this point, we suggest that **INT** is a Ni^{II} species with a bound H_2 molecule. To close a synthetic cycle, zero-valent **1** can be regenerated by adding two equivalents of KC_8 to a THF solution of $\mathbf{3}^{2+}$, upon which a new H_2 evolution cycle can start (Figure 2).

DFT calculations were undertaken to establish a reaction mechanism and to reveal the molecular structure of **INT**. The reaction profile in Figure 3 was calculated at the TPSSh–D4(SMD=MeCN)/def2-TZVPP//r^{2}SCAN-3c level of theory (for r^{2}SCAN-3c, PBE, PBE0 see Figures S44, S45). Starting with the Ni^0 complex **1** and ending up with the Ni^{II} hydride $\mathbf{2}^+$ asserts that protonation in the two proposed positions is feasible, specifically equatorial and axial to the Ni-carbene plane. The equatorial position appears more favorable (ΔG =

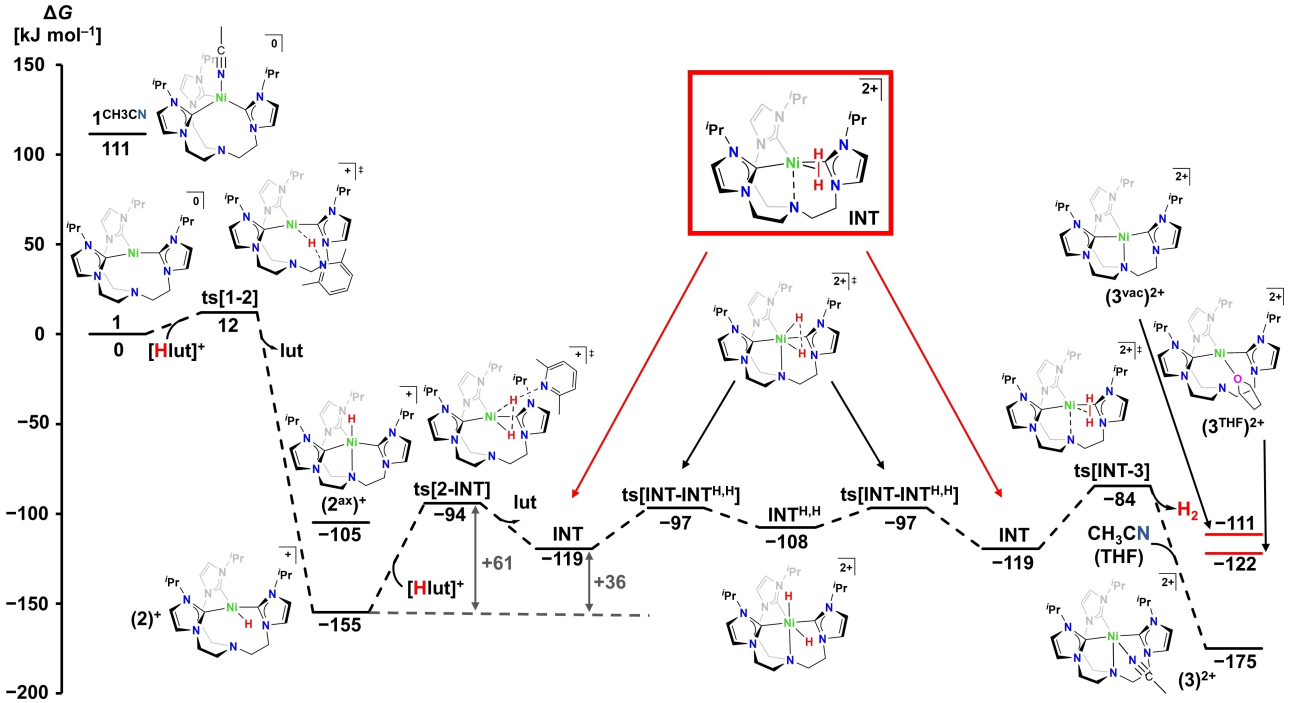

Figure 3. Energy profile obtained at the TPSSh–D4(SMD=MeCN)/def2-TZVPP//r^{2}SCAN-3c level of theory. Compounds $(\mathbf{3}^{THF})^{2+}$ and $(\mathbf{3}^{vac})^{2+}$ relate to the reaction in THF (SMD=THF) with and without coordination of one solvent molecule. For further isomers, see Figure S49.

$-155\ kJ\,mol^{-1}$ for $\mathbf{2}^{+}$ *vs.* $\Delta G = -105\ kJ\,mol^{-1}$ for $(\mathbf{2}^{ax})^{+}$). Whereas the potential energy surface is flat (Figure S47), the second protonation proceeds, consistent with a slow reaction in the cold, with an estimated barrier of $\Delta G^{\ddagger} = +61\ kJ\,mol^{-1} = +155 - 94\ kJ\,mol^{-1}$. With regard to the Ni^{II}–H_2 complex, **INT** ($\Delta G = -119\ kJ\,mol^{-1}$), the computational analyses reveal that the H_2 molecule binds perpendicular to the Ni-carbene plane, slightly raised upwards. Seemingly contradictory to the experiment, the formation of **INT** is predicted to be slightly uphill ($\Delta G = +36 = -119 + 155$) $kJ\,mol^{-1}$. This ambiguity is likely due to computational shortcomings of the implicit solvation model (Figure S48) to properly treat low-coordinate neutral, monocationic, as well as dicationic species.[40] Notably, **INT** is predicted to stand in equilibrium ($\Delta G = +119 - 108 = +1\ kJ$; $\Delta G^{\ddagger} = +22\ kJ\,mol^{-1} = -97 + 119\ kJ\,mol^{-1}$) with the dihydrido complex $\mathbf{INT}^{H,H}$. Intrinsic bond orbitals (IBOs)[41] for the latter, formally tetravalent nickel complex (Figures S55 and S56), suggest an inverted ligand field,[42] thus lowering the metal's oxidation state. Such inverted ligand fields have been likewise proposed for nickel alkyl complexes with a formal Ni^{IV} valence state.[43–45] Scalar-relativistic DFT computations did not allow to distinguish between **INT** and $\mathbf{INT}^{H,H}$ based on the computed ^1H NMR shifts. However, note that **INT** and $\mathbf{INT}^{H,H}$ should, in any case, swiftly interconvert at the NMR timescale (calculated half-life for $\Delta G^{\ddagger} = +22\ kJ\,mol^{-1}$ at $-80\,^{\circ}C$ based on first-order kinetics: $\approx 0.1\ \mu s$). Dihydrogen release proceeds with a low barrier ($\Delta G^{\ddagger} = +71\ kJ\,mol^{-1} = -84 + 155\ kJ\,mol^{-1}$) and, in principle, is reversible in THF ($\Delta G = -122\ kJ\,mol^{-1}$); however, the coordination of the stronger donating acetonitrile renders this elementary step irreversible ($\Delta G = -175\ kJ\,mol^{-1}$).

In the sight of scarce reports on Ni^{II} dihydrogen complexes, the computed structure of **INT** was analyzed in more detail (Figure 4, top). The computed H–H bond length of 0.83 Å is moderately longer than that in free H_2 (0.74 Å). Dihydrogen complexes with H–H bond lengths between 0.8–1.0 Å are commonly referred to as "Kubas-type" complexes.[46–47] Still, nickel dihydrogen complexes are uncommon, and, to date and to the best of our knowledge, only a few of them have been reported.[48–53] In 2012, Heinekey and co-workers reported the first sc-XRD data for a structure with H_2 coordinated to a square planar Ni^{II} center ($d_{H-H} = 0.92$ Å, determined by NMR spectroscopy).[49] In 2012,[52] Peters and co-workers reported a thermally stable Ni^{II}–H_2 complex (DFT: $d_{H-H} = 0.816$ and 0.810 Å for *i*Pr and Ph groups in *tris*-phosphinosilyl ligands) and, later, the first d^{10} Ni–H_2 compound ($d_{H-H} = 0.827$ Å, by NMR studies).[53] In 2015, and later in 2019 and 2020, Lu and co-workers reported hetero-dinuclear In–Ni–H_2 ($d_{H-H} = 0.80(2)$ Å, by NMR, and 0.92(3) Å by XRD studies) and Ga–Ni–H_2 complexes ($d_{H-H} = 0.86$ Å, by NMR studies).[22,50,51] Computationally elucidated, transient examples feature similar H–H bond distances (e.g., for truncated model systems of bis-phosphine ligands: $d_{H-H} \approx 0.90$ Å).[54] We also performed several ^1H NMR measurements to identify proper reaction conditions to measure the relaxation time (T_1)[55] of the H_2 resonance. The only conditions to observe **INT** are shown in the reaction sequence shown in Figures S28 and S29, and described as follows: Starting from [Ni(TIMEN^{iPr})] (**1**), the addition of the proton source in the THF solvent yields the hydride complex $[(TIMEN^{iPr})Ni(H)]^{+}$, $\mathbf{2}^{+}$. Subsequently, the hydride $\mathbf{2}^{+}$ rapidly reacts with another equiv. of H^{+} to form the intermediate H_2 complex, **INT**, that swiftly releases H_2 and gives the sparsely soluble Ni^{II} species $[(TIMEN^{iPr})Ni(NCCH_3)]$, $\mathbf{3}^{2+}$, which precipitates. Thus, conditions that provide a sufficient and constant concentration of the Ni^{II}–H_2 complex, **INT**, could not be achieved.

We conclude that H–H bond activation in **INT** is weak, thus, further rationalizing its transient nature. Indeed, analyzing the canonical molecular orbitals in **INT** (r^2SCAN-3c) corroborates a weak σ-bonding interaction with the formally vacant $d_{x^2-y^2}$ orbital, buried in the HOMO−59 (Figure 4, bottom left; Figures S50 and S51). π-Backbonding by the d_{xz} orbital with the H_2 ligand, which is not well aligned along the *z*-axis and, thus, also allows for small overlap with the d_{yz} orbital (Figures S52 and S53), is likewise weak (Figure 4, bottom right). Energy-decomposition analysis, using natural orbitals for chemical valence (EDA-NOCV) with the TPSSh functional (Figure S54), estimates the stabilization by these two orbital interactions at merely $-92\ kJ\,mol^{-1}$ (σ-bonding) and $-38\ kJ\,mol^{-1}$ (π-backbonding).

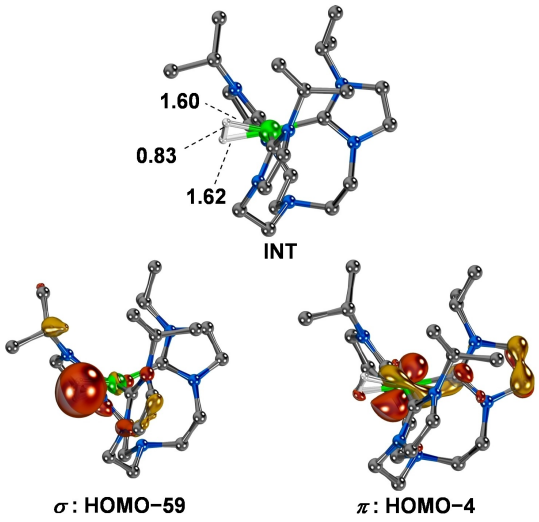

Figure 4. Computed structural parameters of **INT** (top); calculated bond lengths are given in [Å]. σ-Bonding (HOMO − 59, bottom left) and π-backbonding interactions (HOMO − 4, bottom right) in **INT**.

Conclusions

In conclusion, this study reports the synthesis, characterization, and reactivity of the *tris*-N-heterocyclic carbene nickel complex [Ni(TIMEN^{iPr})] (**1**). Zero-valent **1** was assessed for H_2 evolution through protonation with lutidinium salts. The products from two protonation steps, the Ni^{II} hydride $[(TIMEN^{iPr})NiH]^{+}$, $\mathbf{2}^{+}$, and acetonitrile complex $[(TIMEN^{iPr})Ni(NCCH_3)]^{2+}$, $\mathbf{3}^{2+}$, were isolated and characterized. The formation of H_2 was verified by ^1H NMR spectroscopy and quantified by GC-TCD. A low-temperature ^1H NMR study suggested the formation of a rare nickel dihydrogen intermediate, namely $[(TIMEN^{iPr})Ni(H_2)]^{2+}$ (**INT**), which was identified by a characteristic ^1H NMR resonance at −22.3 ppm.

DFT calculations proposed a reaction profile and the molecular structure of **INT**, establishing a weak interaction between the Ni center and the H–H bond. Current and future efforts will focus on the (electro-)catalytic generation of H_2 from Ni-based NHC complexes.

Experimental Section

Details about the characterization methods, including NMR spectroscopy, gas chromatography, cyclic voltammetry, IR vibrational, UV/vis electronic absorption spectroscopy, single-crystal X-ray crystallographic data, and computational details are presented in the Supporting Information.

Deposition Numbers 2235581 (for **1**), 2235582 (for **2** (PF_6)), and 2235583 (for **3** ($BPh_4)_2$) contain the supplementary crystallographic data for this paper. These data are provided free of charge by the joint Cambridge Crystallographic Data Centre and Fachinformationszentrum Karlsruhe Access Structures service.

Synthesis of [Ni(TIMEN^{iPr})] (1): TIMEN^{iPr} (243 mg, 0.571 mmol) was added to a cold suspension of $Ni(COD)_2$ (141 mg, 0.514 mmol) in 5 mL THF, and the color turns red immediately. The solution was stirred for one hour and the solvent was evaporated. The red powder was achieved with extraction from the crude product using 3 mL of diethyl ether and *n*-hexane, each. Yield: 184 mg, 0.380 mmol, 74%. Elemental analysis calcd. (%) for $C_{24}H_{39}N_7Ni$: C 59.52, H 8.12, N 20.24; found: C 59.67, H 8.24, N 20.11.

Synthesis of [(TIMEN^{iPr})Ni(H)](BPh$_4$), (2 (BPh$_4$)): [2,6-Lutidinium](BPh$_4$) (49 mg, 0.114 mmol) was added to a cold solution of Ni(TIMEN^{iPr}) (55 mg, 0.114 mmol) in 5 mL of THF, and the color changes to yellow immediately. After 1 h of stirring, THF was reduced by evaporation, and Et_2O was added to the solution. The yellow precipitate was filtered and washed with Et_2O and *n*-pentane. Yield: 88 mg, 0.109 mmol, 96%. **[(TIMEN^{iPr})Ni(H)](PF$_6$) (2 (PF$_6$))**: $Ni(COD)_2$ (109 mg, 0.396 mmol) was dissolved in 3 mL of THF and added to a suspension of $[H_3TIMEN^{iPr}](PF_6)_3$ (340 mg, 0.394 mmol) in THF. KO*t*Bu (88 mg, 0.784 mmol) was dissolved in 2 mL of THF as well and added dropwise to the suspension. Yield: 201 mg, 0.319 mmol, 81%. Elemental analysis calcd. (%) for $C_{24}H_{40}F_6N_7NiP$: C 45.74, H 6.40, N 15.56; found: C 44.91, H 5.85, N 14.99.

Synthesis of [(TIMEN^{iPr})Ni(NCCH$_3$)](BPh$_4$)$_2$ (3 (BPh$_4$)$_2$): [2,6-Lutidinium](BPh$_4$) (70 mg, 0.164 mmol) was added to a cold solution of [Ni(TIMEN^{iPr})] (36 mg, 0.074 mmol) in 5 mL of THF and the color changes to yellow immediately. After 1 h of stirring, THF was reduced by evaporation, and Et_2O was added to the solution. The yellow precipitate was filtered and washed with Et_2O and *n*-pentane. The yellow crystalline material was obtained from an acetonitrile solution at room temperature. Yield: 81 mg, 0.072 mmol, 97%. **[(TIMEN^{iPr})Ni(NCCH$_3$)](PF$_6$)(BPh$_4$) (3 (PF$_6$)(BPh$_4$))**: [2,6-lutidinium](BPh$_4$) (29 mg, 0.068 mmol) was added to a cold solution of [(TIMEN^{iPr})Ni(H)](PF$_6$) (35 mg, 0.055 mmol) in 5 mL of CH_3CN. After 1 h of stirring, acetonitrile was reduced by evaporation, and yellow crystalline material was obtained from the solution at room temperature. Yield: 50 mg, 0.053 mmol, 96%. Elemental analysis calcd. (%) for $C_{74}H_{82}B_2N_8Ni$: C 76.37, H 7.10, N 9.63; found: C 75.91, H 7.19, N 9.49.

Acknowledgements

This work was funded by the Bundesministerium für Bildung und Forschung (MANGAN and PrometH_2eus, BMBF support codes 03SF0502 and 03HY105I), the Deutsche Forschungsgemeinschaft (DFG, German Research Foundation) – Project-ID 431791331 – SFB 1452 (CLINT Catalysis at Liquid Interfaces), and the Friedrich-Alexander-Universität Erlangen-Nürnberg (FAU). The authors gratefully acknowledge the scientific support and HPC resources provided by the Erlangen National High-Performance Computing Center (NHR@FAU) of the FAU under the NHR project n100af. NHR funding is provided by federal and Bavarian state authorities. NHR@FAU hardware is partially funded by the German Research Foundation (DFG) – 440719683. D.M. thanks the German-American Fulbright Commission for their support. Open Access funding enabled and organized by Projekt DEAL.

Conflict of Interests

The authors declare no conflict of interest.

Data Availability Statement

The data that support the findings of this study are available in the supplementary material of this article.

Keywords: nickel complexes · nickel hydride · nickel dihydrogen · H_2 evolution · NHC

[1] S. van Renssen, *Nat. Clim. Change* **2020**, *10*, 799–801.
[2] N. S. Lewis, D. G. Nocera, *Proc. Natl. Acad. Sci. USA* **2006**, *103*, 15729–15735.
[3] Z. Chen, D. Higgins, A. Yu, L. Zhang, J. Zhang, *Energy Environ. Sci.* **2011**, *4*, 3167–3192.
[4] R. M. Bullock, A. M. Appel, M. L. Helm, *Chem. Commun.* **2014**, *50*, 3125–3143.
[5] P. Connolly, J. H. Espenson, *Inorg. Chem.* **1986**, *25*, 2684–2688.
[6] X. Hu, B. M. Cossairt, B. S. Brunschwig, N. S. Lewis, J. C. Peters, *Chem. Commun.* **2005**, 4723–4725.
[7] X. Hu, B. S. Brunschwig, J. C. Peters, *J. Am. Chem. Soc.* **2007**, *129*, 8988–8998.
[8] J. L. Dempsey, B. S. Brunschwig, J. R. Winkler, H. B. Gray, *Acc. Chem. Res.* **2009**, *42*, 1995–2004.
[9] V. Artero, M. Chavarot-Kerlidou, M. Fontecave, *Angew. Chem. Int. Ed.* **2011**, *50*, 7238–7266.
[10] S. M. Laga, J. D. Blakemore, L. M. Henling, B. S. Brunschwig, H. B. Gray, *Inorg. Chem.* **2014**, *53*, 12668–12670.
[11] N. Kaeffer, M. Chavarot-Kerlidou, V. Artero, *Acc. Chem. Res.* **2015**, *48*, 1286–1295.
[12] S. Todisco, L. Luconi, G. Giambastiani, A. Rossin, M. Peruzzini, I. E. Golub, O. A. Filippov, N. V. Belkova, E. S. Shubina, *Inorg. Chem.* **2017**, *56*, 4296–4307.
[13] N. Queyriaux, D. Sun, J. Fize, J. Pécaut, M. J. Field, M. Chavarot-Kerlidou, V. Artero, *J. Am. Chem. Soc.* **2020**, *142*, 274–282.
[14] M. V. Vollmer, J. Ye, J. C. Linehan, B. J. Graziano, A. Preston, E. S. Wiedner, C. C. Lu, *ACS Catal.* **2020**, *10*, 2459–2470.
[15] M. Wilken, I. Siewert, *ChemElectroChem* **2020**, *7*, 217–221.
[16] K. Schlenker, L. K. Casselman, R. T. VanderLinden, C. T. Saouma, *Catal. Sci. Technol.* **2023**, *13*, 1358–1368.
[17] W. Drinkard, D. Eaton, J. Jesson, R. Lindsey Jr., *Inorg. Chem.* **1970**, *9*, 392–394.

[18] R. Schunn, *Inorg. Chem.* **1970**, *9*, 394–395.
[19] C. A. Tolman, *Inorg. Chem.* **1972**, *11*, 3128–3129.
[20] R. Schunn, *Inorg. Chem.* **1976**, *15*, 208–212.
[21] P. Rigo, M. Bressan, M. Basato, *Inorg. Chem.* **1979**, *18*, 860–863.
[22] R. C. Cammarota, C. C. Lu, *J. Am. Chem. Soc.* **2015**, *137*, 12486–12489.
[23] R. H. Morris, *Chem. Rev.* **2016**, *116*, 8588–8654.
[24] C. J. Curtis, A. Miedaner, W. W. Ellis, D. L. DuBois, *J. Am. Chem. Soc. Rev.* **2002**, *124*, 1918–1925.
[25] W. W. Ellis, R. Ciancanelli, S. M. Miller, J. W. Raebiger, M. Rakowski DuBois, D. L. DuBois, *J. Am. Chem. Soc.* **2003**, *125*, 12230–12236.
[26] C. J. Curtis, A. Miedaner, J. W. Raebiger, D. L. DuBois, *Organometallics* **2004**, *23*, 511–516.
[27] N. A. Eberhardt, H. Guan, *Chem. Rev.* **2016**, *116*, 8373–8426.
[28] R. E. Adams, T. A. Grusenmeyer, A. L. Griffith, R. H. Schmehl, *Coord. Chem. Rev.* **2018**, *362*, 44–53.
[29] N. V. Belkova, L. M. Epstein, O. A. Filippov, E. S. Shubina, *Chem. Rev.* **2016**, *116*, 8545–8587.
[30] S. C. Robinson, D. Heinekey, *Chem. Commun.* **2017**, *53*, 669–676.
[31] S. Amanullah, P. Saha, A. Nayek, M. E. Ahmed, A. Dey, *Chem. Soc. Rev.* **2021**, *50*, 3755–3823.
[32] N. V. Kireev, A. S. Kiryutin, A. A. Pavlov, A. V. Yurkovskaya, E. I. Musina, A. A. Karasik, E. S. Shubina, K. L. Ivanov, N. V. Belkova, *Eur. J. Inorg. Chem.* **2021**, 4265–4272.
[33] R. C. Cammarota, L. J. Clouston, C. C. Lu, *Coord. Chem. Rev.* **2017**, *334*, 100–111.
[34] D.-H. Manz, P.-C. Duan, S. Dechert, S. Demeshko, R. Oswald, M. John, R. A. Mata, F. Meyer, *J. Am. Chem. Soc.* **2017**, *139*, 16720–16731.
[35] D. Schilter, J. M. Camara, M. T. Huynh, S. Hammes-Schiffer, T. B. Rauchfuss, *Chem. Rev.* **2016**, *116*, 8693–8749.
[36] X. Hu, I. Castro-Rodriguez, K. Meyer, *Chem. Commun.* **2004**, 2164–2165.
[37] L. Yang, D. R. Powell, R. P. Houser, *Dalton Trans.* **2007**, 955–964.
[38] M. Garçon, C. Bakewell, G. A. Sackman, A. J. White, R. I. Cooper, A. J. Edwards, M. R. Crimmin, *Nature* **2019**, *574*, 390–393.
[39] S. Ramakrishnan, S. Chakraborty, W. W. Brennessel, C. E. Chidsey, W. D. Jones, *Chem. Sci.* **2016**, *7*, 117–127.
[40] D. Munz, D. Meyer, T. Strassner, *Organometallics* **2013**, *32*, 3469–3480.
[41] G. Knizia, *J. Chem. Theory Comput.* **2013**, *9*, 4834–4843.
[42] R. Hoffmann, S. Alvarez, C. Mealli, A. S. Falceto, T. J. Cahill III, T. Zeng, G. Manca, *Chem. Rev.* **2016**, *116*, 8173–8192.
[43] J. S. Steen, G. Knizia, J. E. Klein, *Angew. Chem. Int. Ed.* **2019**, *58*, 13133–13139.
[44] E. C. Kisgeropoulos, A. C. Manesis, H. S. Shafaat, *J. Am. Chem. Soc.* **2021**, *143*, 849–867.
[45] I. M. DiMucci, C. J. Titus, D. Nordlund, J. R. Bour, E. Chong, D. P. Grigas, C.-H. Hu, M. D. Kosobokov, C. D. Martin, L. M. Mirica, *Chem. Sci.* **2023**, *14*, 6915–6929.
[46] G. J. Kubas, R. R. Ryan, B. I. Swanson, P. J. Vergamini, H. J. Wasserman, *J. Am. Chem. Soc.* **1984**, *106*, 451–452.
[47] R. H. Crabtree, *Chem. Rev.* **2016**, *116*, 8750–8769.
[48] T. He, N. P. Tsvetkov, J. G. ino, X. Gao, B. C. Fullmer, K. G. Caulton, *J. Am. Chem. Soc.* **2010**, *132*, 910–911.
[49] S. J. Connelly, A. C. Zimmerman, W. Kaminsky, D. M. Heinekey, *Chem. Eur. J.* **2012**, *18*, 15932–15934.
[50] R. C. Cammarota, J. Xie, S. A. Burgess, M. V. Vollmer, K. D. Vogiatzis, J. Ye, J. C. Linehan, A. M. Appel, C. Hoffmann, X. Wang, V. G. Young, C. C. Lu, *Chem. Sci.* **2019**, *10*, 7029–7042.
[51] B. L. Ramirez, C. C. Lu, *J. Am. Chem. Soc.* **2020**, *142*, 5396–5407.
[52] C. Tsay, J. C. Peters, *Chem. Sci.* **2012**, *3*, 1313–1318.
[53] W. H. Harman, T. P. Lin, J. C. Peters, *Angew. Chem. Int. Ed.* **2014**, *53*, 1081–1086.
[54] C. Flener Lovitt, G. Frenking, G. S. Girolami, *Organometallics* **2012**, *31*, 4122–4132.
[55] P. J. Desrosiers, L. Cai, Z. Lin, R. Richards, J. Halpern, *J. Am. Chem. Soc.* **1991**, *113*, 4173–4184.

Manuscript received: June 29, 2023
Accepted manuscript online: August 24, 2023
Version of record online: October 6, 2023